The Role of the Mindoro–Sibutu Pathway on the South China Sea Multilayer Circulation

MINGTING LI,[a,b] HUIJIE XUE,[c,d] JUN WEI,[a,b] LINLIN LIANG,[c] ARNOLD L. GORDON,[e] AND SONG YANG[a,b]

[a] *School of Atmospheric Sciences, Sun Yat-sen University, and Guangdong Province Key Laboratory for Climate Change and Natural Disaster Studies, Zhuhai, China*
[b] *Southern Marine Science and Engineering Guangdong Laboratory, Zhuhai, China*
[c] *State Key Laboratory of Tropical Oceanography, South China Sea Institute of Oceanology, Chinese Academy of Sciences, Guangzhou, China*
[d] *School of Marine Sciences, University of Maine, Orono, Maine*
[e] *Lamont-Doherty Earth Observatory, Columbia University, Palisades, New York*

(Manuscript received 21 July 2020, in final form 27 May 2021)

ABSTRACT: The role of the Mindoro Strait–Sibutu Passage pathway in influencing the Luzon Strait inflow to the South China Sea (SCS) and the SCS multilayer circulation is investigated with a high-resolution ($0.1° \times 0.1°$) regional ocean model. Significant changes are evident in the SCS upper-layer circulation (250–900 m) by closing the Mindoro–Sibutu pathway in sensitivity experiments, as Luzon Strait transport is reduced by 75%, from −4.4 to −1.2 Sv ($1\ \text{Sv} \equiv 10^6\ \text{m}^3\ \text{s}^{-1}$). Because of the vertical coupling between the upper and middle layers, closing the Mindoro–Sibutu pathway also weakens clockwise circulation in the middle layer (900–2150 m), but there is no significant change in the deep layer (below 2150 m). The Mindoro–Sibutu pathway is an important branch of the SCS throughflow into the Indonesian Seas. It is also the gateway for oceanic waves propagating clockwise around the Philippines Archipelago from the western Pacific Ocean into the eastern SCS, projecting El Niño–Southern Oscillation sea level signals to the SCS, impacting its interannual variations and multilayer circulation. The results provide insights into the dynamics of how upstream and downstream passage throughflows are coupled to affect the general circulation in marginal seas.

KEYWORDS: Ocean circulation; Ocean models; Waves, oceanic; Transport; Interannual variability

1. Introduction

The South China Sea (SCS), extending from 5° to 25°N and from 100° to 120°E, is the largest marginal sea in the western North Pacific Ocean. In the north, the SCS connects to the East China Sea through Taiwan Strait and to the western Pacific Ocean through Luzon Strait. In the south, the SCS connects to the Java Sea via Karimata Strait and to the Sulu Sea via Mindoro Strait. The latter continues to the Sulawesi Sea via the Sibutu Passage (Fig. 1). The circulation of the SCS is mainly driven by the East Asian monsoon (e.g., Xue et al. 2004; Gan et al. 2006, and references therein). Cyclonic circulation occurs in winter northeast monsoon, shifting to an anticyclonic or a dipole pattern during summer when the southwest monsoon prevails. The SCS throughflow, originating from Kuroshio intrusion through Luzon Strait and flowing into the Indonesian Seas through Karimata Strait and Mindoro Strait–Sibutu Passage, is a major constituent of the SCS general circulation (Qu et al. 2006; Fang et al. 2010; Susanto et al. 2013; Wei et al. 2016), transporting heat and freshwater across the SCS (Qu 2000; Wang et al. 2006; Qu et al. 2006, 2009) and impacting the Indonesian Throughflow (Qu et al. 2005; Wang et al. 2006; Tozuka et al. 2009; Qu et al. 2009; Du and Qu 2010; Liu et al. 2012; Gordon et al. 2012; Wei et al. 2016). As such the SCS throughflow is one of the key pathways for water exchanges between the Pacific and the Indian Oceans (Metzger and Hurlburt 1996; Tozuka et al. 2009; Gordon et al. 2012).

Driven by the East Asian monsoon and Kuroshio intrusion, combined with topographic effects and interior dynamical adjustment, the SCS displays a depth-dependent circulation, composed of a cyclonic–anticyclonic–cyclonic circulation pattern (Yuan 2002; Shu et al. 2014; Xu and Oey 2014; Lan et al. 2015; Gan et al. 2016; Cai and Gan 2019; Quan and Xue 2019; Zhu et al. 2019; Cai et al. 2020). The upper and deep layers exhibit cyclonic circulation, while the middle layer is characterized by anticyclonic circulation. The upper layer from the surface to about the 750-m depth can be divided into surface and subsurface layers, with the surface layer (<200 m) circulation driven predominantly by the monsoonal winds (e.g., Wyrtki 1961; Chu et al. 1999; Hu et al. 2000; Liu et al. 2001), displaying seasonal variations that is cyclonic in winter and a dipole circulation (anticyclonic in the south and cyclonic in the north) in summer (e.g., Su 2004; D. Wang et al. 2006; G. Wang et al. 2006; Quan et al. 2016; Gan et al. 2016; Zu et al. 2019, 2020). The cyclonic circulation of the subsurface layer (200–750 m) is driven by Ekman pumping and the Kuroshio intrusion through Luzon Strait (Xue et al. 2004; Gan et al. 2016; Quan and Xue 2018; Cai et al. 2020).

Contemporary studies on the basin-scale middle- and deep-layer circulation, mostly based on diagnosis results of models and hydrographic data due to lack of direct observations (Tian and Qu 2012; Wang et al. 2019), indicate that the deep-layer (below ~2000 m) circulation of the SCS is cyclonic (Wang et al. 2011; Xu and Oey 2014; Shu et al. 2014; Zhu et al. 2017). Some

Supplemental information related to this paper is available at the Journals Online website: https://doi.org/10.1175/JPO-D-20-0165.s1.

Corresponding author: Huijie Xue, huijiexue@scsio.ac.cn

DOI: 10.1175/JPO-D-20-0165.1

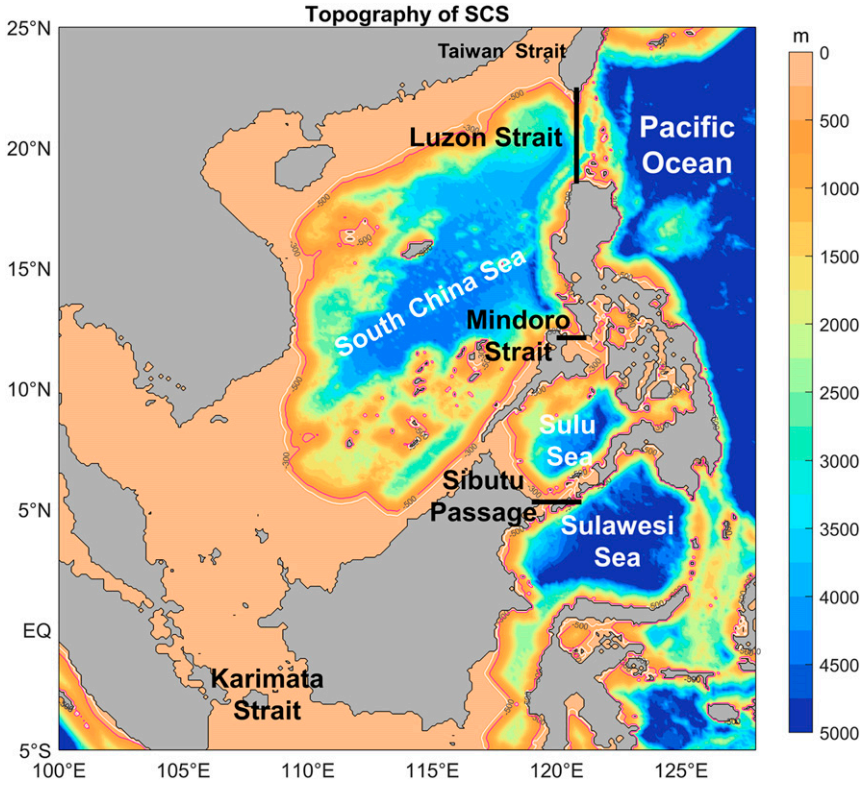

FIG. 1. Topography of the SCS region as based on the ATOP model with key straits (Luzon Strait, Mindoro Strait, Sibutu Passage, Karimata Strait, and Taiwan Strait) marked. The shaded areas represent the depth (m) of the ocean. The white and red curves indicate 300- and 500-m-depth isobaths. Black lines show sections used in the analysis and sensitivity experiments.

studies (e.g., Lan et al. 2013; Gan et al. 2016; Cai et al. 2020) suggested that the deep-layer cyclonic circulation from about 2000 m to the bottom is driven by deep-water ventilation derived from Luzon Strait inflow, while Quan and Xue (2019) demonstrated that the abyssal mixing in the SCS plays an essential role in modulating pressure gradient that drives Luzon Strait overflow and the deep cyclonic circulation. The middle layer (750–2000 m) anticyclonic circulation is driven by interaction with the upper and deep layers through vertical coupling and vorticity flux (Gan et al. 2016; Quan and Xue 2018; Cai and Gan 2019; Quan and Xue 2019; Cai et al. 2020).

The Luzon Strait, with a sill depth about 2400 m, is the only deep channel between the SCS and western Pacific Ocean, and plays a crucial role in the formation of the multilayer circulation in the SCS (Xue et al. 2004; Nan et al. 2011; Lan et al. 2013; Quan and Xue 2019). The Luzon Strait throughflow provides vorticity flux into the SCS driving its multilayer circulation (Xu and Oey 2014; Gan et al. 2016; Cai et al. 2020). Based on observations and models, many studies have indicated that the mean transport of Luzon Strait is westward at 2–6 Sv ($1\ \text{Sv} \equiv 10^6\ \text{m}^3\ \text{s}^{-1}$) with significant seasonal and interannual variability (Tian et al. 2006; Nan et al. 2015; Quan et al. 2016). The Luzon Strait inflow is stronger during winter and El Niño, and weaker during summer and La Niña (Qu et al. 2004; Tsui and Wu 2012; Gordon et al. 2012).

The Mindoro Strait (sill depth of ~500 m) and Sibutu Passage (sill depth of ~300 m) are the key narrow straits in the Philippine Archipelago, which connect the SCS and Indonesian Seas where outflows from the SCS to the Indonesian Seas occur in the subsurface layer. Many studies have pointed out the importance of the Philippine Archipelago to the regional circulation and climate system (Gordon et al. 2011; Gordon and Villanoy 2011; Sprintall et al. 2012). The Philippine Archipelago, located at the nexus of the El Niño–Southern Oscillation (ENSO) and the Asian monsoon, connects the western marginal seas to the tropical Pacific Ocean forming a unique environment. The complex geography of the islands, seas, and straits of the region poses challenges to both observation and modeling. The Philippine Straits Dynamics Experiment (PhilEx) project during 2007–09 integrated in situ and remote observations with models, which advanced our understanding of the oceanic dynamics and water exchanges in the Philippine Archipelago (Gordon et al. 2011; Gordon and Villanoy 2011). Moored sensors during the PhilEx project provide a time series of the velocity profile within Mindoro Strait (Sprintall et al. 2012), finding that the southward mean transport was 0.1 Sv in 2008, with occasionally attaining southward transport of 1–2 Sv. There is no observation as yet in the Sibutu Passage. Model simulations and remotely sensed altimetric measurements suggested a mean southward transport in Mindoro Strait ranging from ~0.5 Sv to

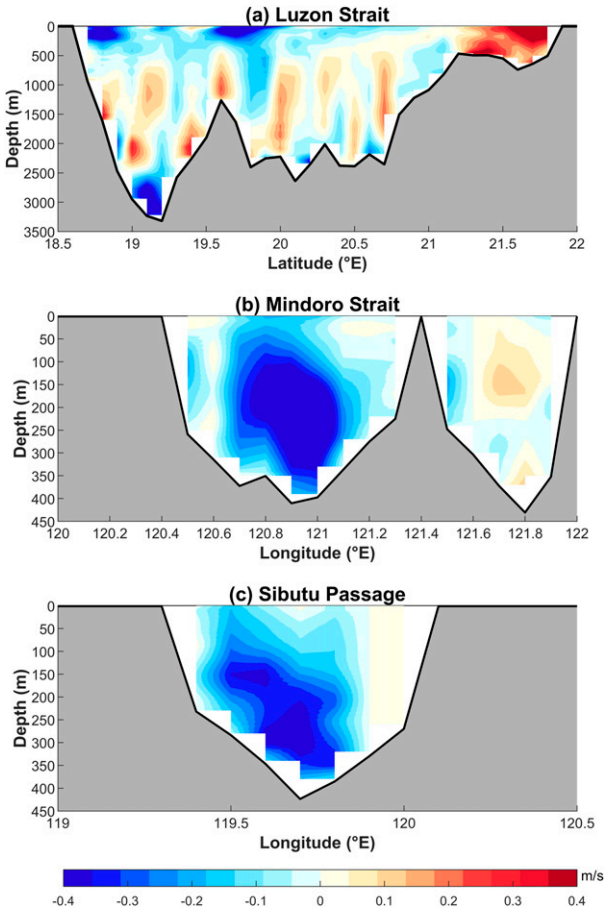

FIG. 2. Cross section of the mean flow from the model (averaged from 2008 to 2016) through the Luzon Strait (zonal) at (a) 120.8°E, (b) Mindoro Strait (meridional) at 12.1°N, and (c) Sibutu Passage (meridional) at 5.3°N. The negative values represent westward flow in (a) but southward flow in (b) and (c). The mean transport (2008–16) through Luzon Strait is westward at 4.4 Sv, and the mean transport through Mindoro Strait and Sibutu Passage is southward at 2.7 and 2.9 Sv, respectively.

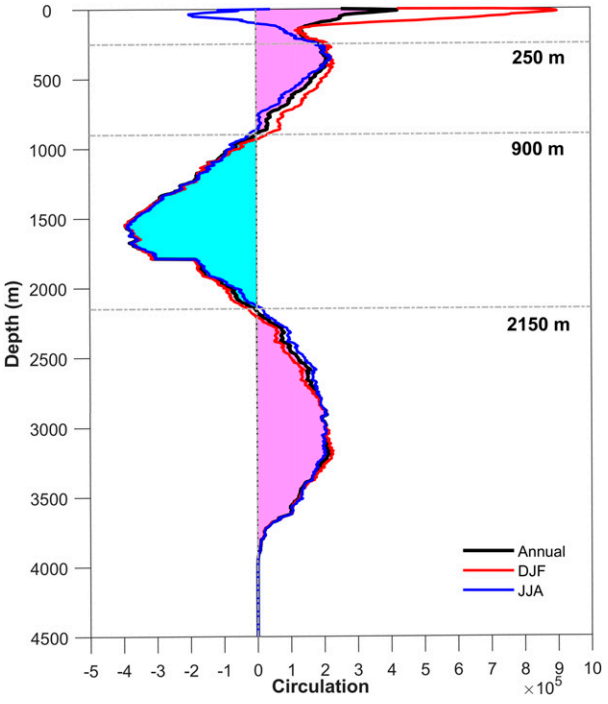

FIG. 3. The SCS basin (coastline in region of 5°–22°N and 105°–121°E) integrated vorticity is based on Eq. (1) as a function of depth from the control run. The mean (from 2008 to 2016) profile of annual, December–February, and June–August is shown by the thick black, red, and blue solid lines, respectively. The light-purple shading represents the cyclonic circulation of 9-yr mean, and the cyan shading represents the anticyclonic circulation.

4 Sv, and similarly for the Sibutu Passage (Metzger and Hurlburt 1996; Qu et al. 2006; Qu and Song, 2009; Hurlburt et al. 2011; Gan et al. 2016). The Mindoro–Sibutu pathway is a main outflow channel for the SCS throughflow (Wang et al. 2006; Qu and Song 2009), as both Karimata and Taiwan Strait, shallower than 100 m, involve only the SCS surface layer. Previous studies have indicated that the Mindoro–Sibutu pathway is crucial for the SCS throughflow that interacts with the Indonesian Throughflow (Gordon et al. 2012; Wei et al. 2016; Li et al. 2019).

The Mindoro Strait–Sibutu Passage also provides a pathway for low-frequency oceanic waves that propagate from the western Pacific Ocean into the SCS (Liu et al. 2011; Zhuang et al. 2013; Chen et al. 2015). Liu et al. (2011) suggested that ENSO-related off-equatorial Rossby waves in the western Pacific excite coastal Kelvin waves, which propagate northward along the western margin of the Philippine Archipelago and enter the SCS through Sibutu Passage and then Mindoro Strait. Part of the coastal Kelvin wave energy that enters into the Sulawesi Sea from the western Pacific Ocean can propagate southward along the east Kalimantan coast after bypassing Sibutu Passage (Hu et al. 2019).

Although Luzon Strait is often considered upstream while the Mindoro–Sibutu pathway is downstream in the view of SCS circulation, relative contributions of these two gateways to the SCS circulation and hydrography changes are still unclear. Model sensitivity experiments with closing straits help understand dynamical relationships between straits and circulation (Tozuka et al. 2007; Zhuang et al. 2013). We showed previously that if the Mindoro–Sibutu pathway were closed, the whole-depth volume transport at Luzon Strait would be reduced by about 75%, and the upper-layer circulation particularly the SCS throughflow would become much weaker (Li et al. 2019). A question naturally follows: How does the change induced by closing the Mindoro–Sibutu pathway affect the general multilayer circulation of the SCS as the multilayer circulation is tightly coupled in the vertical (Wang et al. 2012; Quan and Xue 2018, 2019)? Water mass and energy exchanges between the western Pacific Ocean and the SCS through the Luzon Strait can modulate sea level, salinity and temperature changes in the SCS (Xue et al. 2004; Qu et al. 2006; Zhuang et al. 2013). The sea level in the SCS and volume transport through the Mindoro–Sibutu pathway, even the Luzon Strait transport may also be impacted by the ENSO-related coastal Kelvin waves, which needs further examination. A more focused objective of

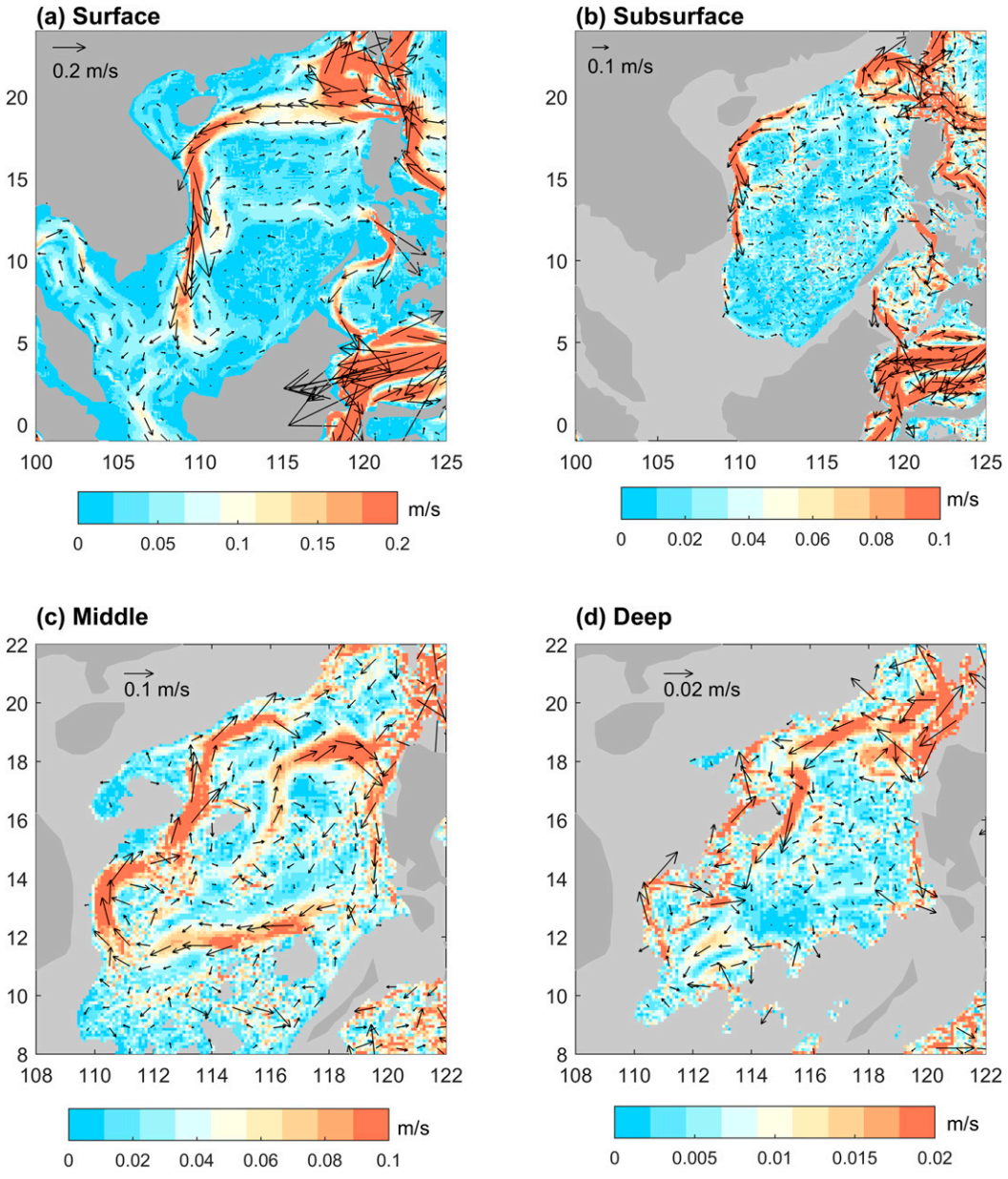

FIG. 4. Multilayer circulation of SCS in the control run. The upper-layer cyclonic circulation including (a) the surface layer averaged from 0 to 250 m and (b) the subsurface layer averaged from 250 to 900 m; (c) the middle-layer anticyclonic circulation averaged from 900 to 2150 m; and (d) the deep-layer cyclonic circulation averaged from 2150 m to the seafloor. Shading represents the velocity magnitude (m s^{-1}). Note that the color bars on the bottom of different panels have different scales.

this study is to provide insights into the dynamics of how upstream and downstream passage throughflows are coupled to affect the general circulation in marginal seas.

Following Li et al. (2019), we conducted several sensitivity experiments by closing Luzon Strait, Sibutu Passage, and both of them to investigate impact of the Mindoro–Sibutu pathway on the SCS multilayer circulation and the Luzon Strait inflow, as well as relative contribution to the SCS sea level changes. The paper is organized as follows. Section 2 gives a brief introduction of regional ocean model and configuration of sensitivity experiments. Section 3 describes results from sensitivity experiments. Summary and discussions are given in section 4.

2. Regional ocean model and sensitivity experiments

The Advanced Taiwan Ocean Prediction (ATOP) regional ocean model, based on the Princeton Ocean Model (POM),

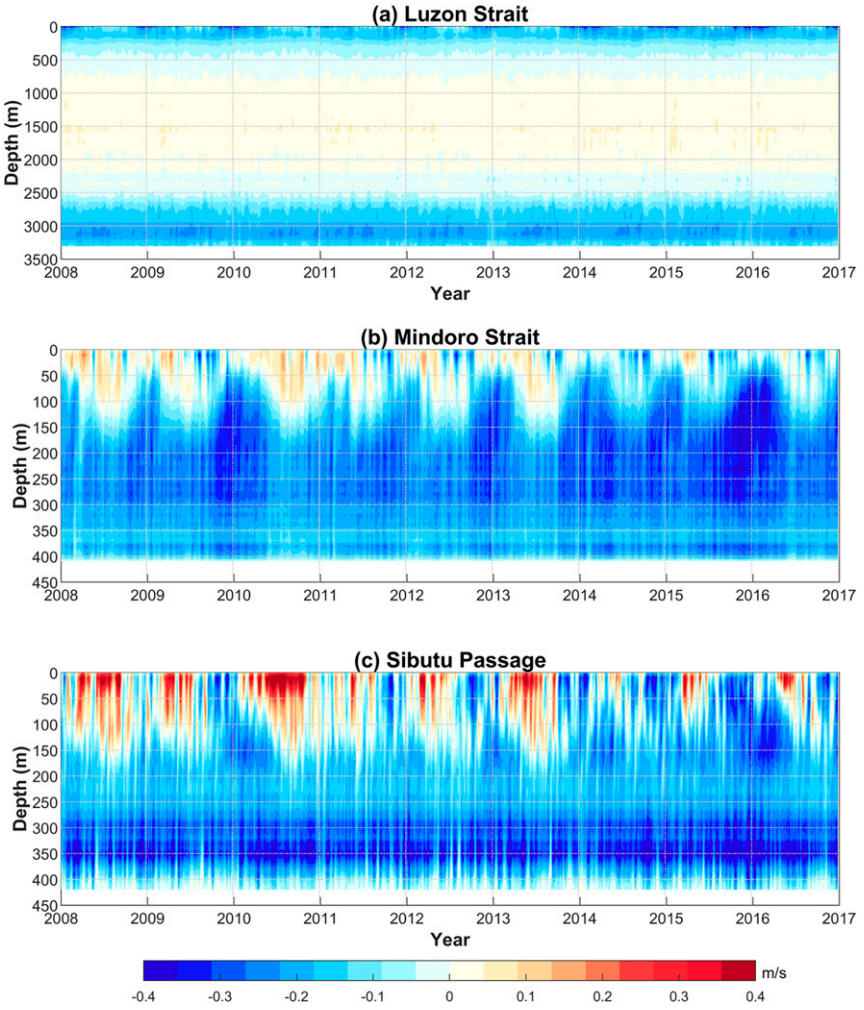

FIG. 5. Time–vertical distribution of mean zonal velocity in (a) Luzon Strait at 120.8 °E and mean meridional velocity at (b) Mindoro Strait at 12.1 °N and (c) Sibutu Passage at 5.3 °N from 2008 to 2016 as based on the control experiment ($m\,s^{-1}$).

was developed by Oey et al. (2013, 2014) for the North Pacific Ocean and had been used for several studies (e.g., Xu and Oey 2014; Wei et al. 2016; Li et al. 2019). The model has a resolution of 0.1° × 0.1° and includes the entire North Pacific Ocean, the "Maritime Continent," and the Indonesian Seas/straits, spanning from 99°E to 70°W and 15°S to 72°N. The model has 41 vertical sigma levels with finer resolution near the surface and ocean bottom. To minimize sigma-level pressure-gradient errors, a fourth-order scheme was used (Berntsen and Oey 2010). The Smagorinsky turbulence closure scheme (Smagorinsky 1963) is applied to calculate horizontal eddy viscosity and diffusivity, while the Mellor and Yamada level-2.5 turbulence closure scheme is used for vertical eddy viscosity and diffusivity (Mellor and Yamada 1982). The only open boundary (south) is forced by the *World Ocean Atlas* (*WOA*) monthly climatological temperature and salinity using a nesting procedure described by Oey and Chen (1992a,b). The model was forced by 6-hourly Cross-Calibrated Multi-Platform (CCMP) winds, which were produced using satellite, moored buoy, and model wind data (Mears et al. 2019), with a resolution of 0.25°. All experiments in this study were started from a restart file of 1 January 2004 from Oey et al. (2014). Outputs of 5-day-averaged variables for all experiments are analyzed. The model properly simulates the western boundary currents system, SCS throughflow and Indonesian Throughflow when comparing model simulations with available observational data, Simple Ocean Data Assimilation (SODA) reanalysis, a 1/12° regional version of the NEMO physical ocean model (INDO12) and Ocean General Circulation Model for the Earth Simulator (OFES) high-resolution model outputs in our previous study (Wei et al. 2016).

Li et al. (2019) conducted a set of sensitivity experiments based on ATOP and showed changes in the upper thermocline layer of the SCS and Indonesian Seas responding to closure of Luzon Strait and the Mindoro–Sibutu pathway, respectively. This study conducted sensitivity experiments by closing Luzon Strait and the Mindoro–Sibutu Pathway to analyze specific impacts of each strait on the SCS multilayer circulation.

Figure 2 shows the cross section of the mean flow from the model through the Luzon Strait, Mindoro Strait and Sibutu Passage. The ATOP model appears to resolve well the critical topographic features in these three key straits. When compared with the 1/25° HYCOM result (Hurlburt et al. 2011), ATOP model produces a similar velocity profile at Mindoro Strait. Three sensitivity experiments are used in this study: Closing Luzon Strait (Luzon_Closed), Closing Sibutu Strait (Sibutu_Closed), and Closing both Luzon and Sibutu Straits (Luzon_Sibutu_Closed). We focus on the Sibutu_Closed experiment as blocking the Sibutu Passage effectively blocks the Mindoro–Sibutu Pathway. The sensitivity experiments were started in January 2004 and continued to December 2016. The mean kinetic energy of the SCS (coastline in region of 5°–22°N and 105°–121°E) in the Sibutu_Closed experiment reached equilibrium after 1–2 years (Fig. S1 in the online supplemental material), and the total volume of SCS after 4 years. The last 9 yr (2008–16) of simulation results were used in following analyses.

3. Results

a. *Multilayer circulation of the SCS*

We define SCS circulation layers following the vertical structure derived from the control run output. The circulation Γ as a function of depth is the domain-integrated vorticity based on the Stokes theorem:

$$\Gamma = \oint_C r\mathbf{u}\cdot\mathbf{l}\,ds = \iint_C \xi\,dA, \tag{1}$$

where Γ is the basin circulation, C represents the basin boundary, r is a linear friction coefficient, $\mathbf{u}$ is the velocity vector, $\mathbf{l}$ is the unit vectors that are parallel to C, ξ is the relative vorticity, and A is the inner area of the SCS basin. Consistent with previous studies, the control run results show a clear cyclonic–anticyclonic–cyclonic circulation with small discrepancies at specific depth (Fig. 3). Based on annual mean pattern averaged from 2008 to 2016, the cyclonic circulation layer occurs in the upper 900 m; the anticyclonic layer is from 900 to 2150 m; and the deep layer is from the 2150-m depth to the sea floor, in which the SCS is isolated from the surrounding ocean, as the sill depth of eastern Luzon Strait is 2000 m in ATOP model. The cyclonic circulation in the upper layer is stronger in winter than in summer, with the upper 120 m marked by anticyclonic circulation in summer. Considering the seasonal variation diminishes at about 250 m, we divide the upper 900 m of the SCS into the surface layer (upper 250 m) and the subsurface layer (250–900 m). The time-averaged SCS basin circulation patterns for four layers are examined in control and sensitivity experiments.

The depth-averaged velocity for 0–250, 250–900, 900–2150, and below 2150 m of the control experiment averaged from January 2008 to December 2016 is shown in Fig. 4. The surface layer cyclonic circulation exhibits strong westward current from Luzon Strait and an eastward current at about 12°N, while the middle layer shows strong westward current around 12°–13°N. The circulation is cyclonic in the surface and subsurface layer, with a clear western boundary current flowing along the slope regions off China and Vietnam (Figs. 4a,b). This western

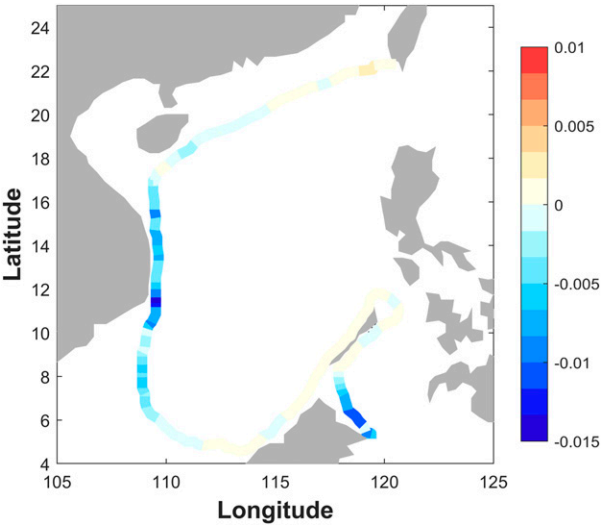

FIG. 6. Time-averaged (2008–16) difference of kinetic energy along the 200-m-depth isobaths between the Sibutu_Closed and control experiments ($m^2\,s^{-2}$). The difference between the Sibutu_Closed and control experiments indicates the results of Sibutu_Closed minus control.

boundary current is induced by basin-scale wind stress and Luzon Strait inflow (Xue et al. 2004; Gan et al. 2006; Quan et al. 2016). Two branches of the SCS throughflow (the Luzon–Karimata and the Luzon–Mindoro–Sibutu throughflow; Li et al. 2019) appear in both layers, forming a circulation system with Luzon Strait representing the upstream and the Mindoro–Sibutu pathway as the downstream. There is an anticyclonic circulation in the middle layer and a cyclonic circulation in the deep layer (Figs. 4c,d). Vertical distributions of the mean velocity in Luzon Strait, Mindoro Strait and Sibutu Passage are shown in Fig. 5. The Luzon Strait presents a clear "sandwich-like" velocity pattern, with westward inflow in the upper and deep layers, while eastward outflow in the middle layer. The flow through the Mindoro–Sibutu pathway is stronger at subsurface depths from 150 to 350 m than that within the surface layer because the surface layer exhibits seasonally reversing flows. The 9-yr (2008–16) mean transport through the Mindoro Strait is southward at 2.7 Sv, and the annual mean for 2008 is 1.5 Sv. The latter is 15 times stronger than the 0.1 Sv reported by Sprintall et al. (2012). Although the mean southward velocities in Mindoro Strait from ATOP model are much stronger than those from the mooring record during PhilEx period in 2008 (Sprintall et al. 2012), the model simulates seasonal and interannual variations consistent with previous studies (Qu and Song 2009; Hurlburt et al. 2011).

Previous studies have explained the formation of SCS multilayer circulation by invoking the potential vorticity integral constraint theory (Yang and Price 2000; Lan et al. 2013; Xu and Oey 2014). As shown in Xu and Oey (2014), the line integral potential vorticity equation over the basin is

$$\oint_C r\mathbf{u}\cdot\mathbf{l}\,ds \approx \oint_C (\tau/H)\cdot\mathbf{l}\,ds - \sum_{i=1}^{N} q_i f_i \big/ H_i, \tag{2}$$

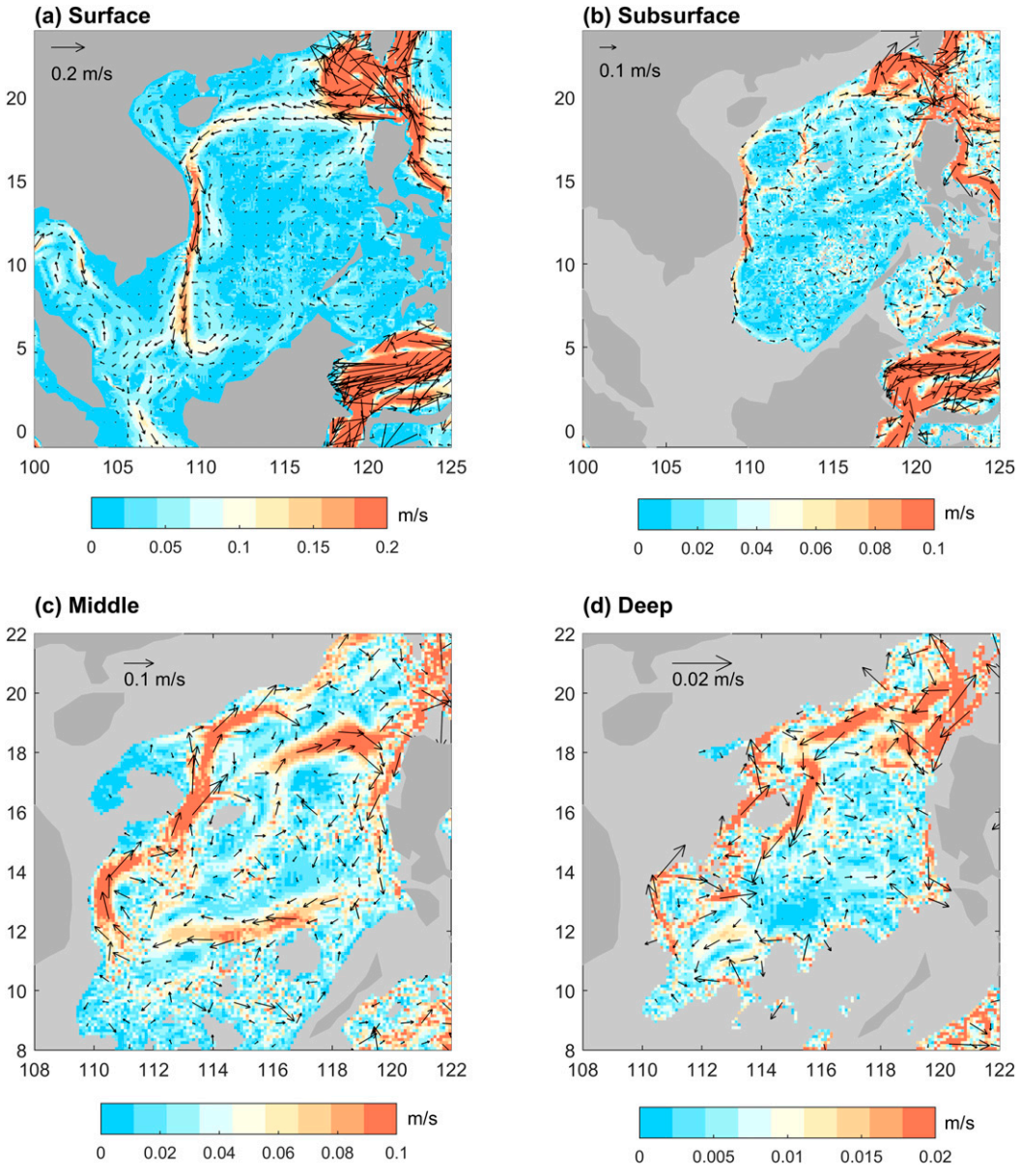

FIG. 7. As in Fig. 4, but for the Sibutu_Closed experiment ($m\,s^{-1}$). Note that the color bars on the bottom of different panels have different scales.

where q_i is the volume transport through the straits and passages in different layers, H_i is the layer thickness, f_i is the Coriolis force, and N represents the number of straits and passages in each layer. For the subsurface layer, Ekman pumping as well as the net contribution of potential vorticity fluxes induce a cyclonic circulation (Qu 2000). There are two openings in subsurface layer: Luzon Strait provides influx, hence $qf/H < 0$, and the Mindoro Strait provides outflux, hence $qf/H > 0$. The H value in Mindoro Strait of subsurface layer is only about 150 m (from 250 m to bottom), while the depth of Luzon Strait is from 250 to 900 m, which is 4.3 times H in Mindoro Strait. Since the depth-integrated transport at Luzon Strait (−3.2 Sv averaged from 2008 to 2016) is nearly 4.6 times that at the Mindoro Strait (−0.7 Sv averaged from 2008 to 2016) and f is larger at the Luzon Strait, the last term of Eq. (2) is positive, which gives rise to a cyclonic basin-scale circulation. As for the middle layer, the eastward Luzon Strait transport contributes to a negative potential vorticity flux and therefore an anticyclonic circulation. The circulation of the deep layer is generally cyclonic, which is induced by the deep-water overflow through the Luzon Strait (Qu et al. 2006; Lan et al. 2013).

b. *Changes of multilater circulation in the Sibutu_Closed experiment*

Closing the Mindoro–Sibutu pathway (Sibutu_Closed experiment) leads to a relatively weaker cyclonic circulation in

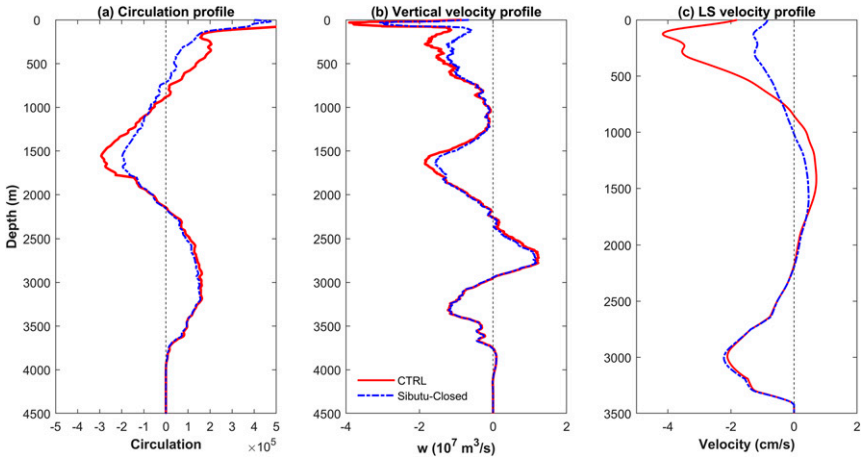

FIG. 8. (a) SCS domain-integrated vorticity, (b) domain-integrated vertical velocity w, and (c) width-averaged zonal current in Luzon Strait as a function of depth from the control experiment (red line) and the Sibutu_Closed sensitivity experiment (blue line) averaged from 2008 to 2016. Positive values represent upward velocities in (b) and eastward velocities in (c).

the surface and subsurface layers in comparison with those in the control experiment. Significant changes of mean kinetic energy are seen along 200-m-depth isobaths in the SCS when the Sibutu_Closed experiment is compared with the control experiment, especially in the Sulu Sea and western boundary current along the Vietnam margin (Fig. 6). The western boundary current of SCS in the subsurface layer is weaker, about half of its counterpart in the control experiment, which implies that the Mindoro–Sibutu pathway plays a role in the formation of the western boundary current (Fig. 7). Combined with the vertical distributions of zonally averaged U and V velocity component anomalies for the entire SCS to its maximum depth (Fig. S2 in the online supplemental material), closing the Mindoro–Sibutu pathway leads to a diminishing eastward current in surface and subsurface layer between 10° and 16°N, as well as weaker westward current anomalies in middle layer at Mindoro Strait latitudes. The meridional velocity in subsurface layer is southward south of 20°N, which reflects the SCS throughflow. Closing the Mindoro–Sibutu pathway, northward anomalies in surface and subsurface layer indicate strong decrease of southward SCS throughflow. Meanwhile, northward current in middle layer is also decreased between 11° and 22°N. The middle-layer outflow in Luzon Strait decreases by about 20% upon closing the Mindoro–Sibutu pathway, indicating that the Mindoro–Sibutu pathway affects both Luzon Strait inflow and multilayer circulation in the SCS. Consistent with velocity patterns, the domain-integrated kinetic energy is also modified, mainly in the surface and subsurface layer (not shown), and it is reduced significantly in the western boundary current and cyclonic current to the Mindoro Strait. The western boundary current in Sibutu_Closed is stronger than that in the Luzon_Closed experiment but is still weaker than that in the control experiment, and it extends to the north of the Sunda Shelf (Fig. S3 in the online supplemental material).

The SCS domain-integrated vorticity, vertical velocity, as well as zonal velocity in Luzon Strait as a function of depth from control run and the Sibutu_Closed sensitivity experiment, are shown in Fig. 8. Although the Mindoro–Sibutu pathway is located in the surface and subsurface layer, the middle layer is

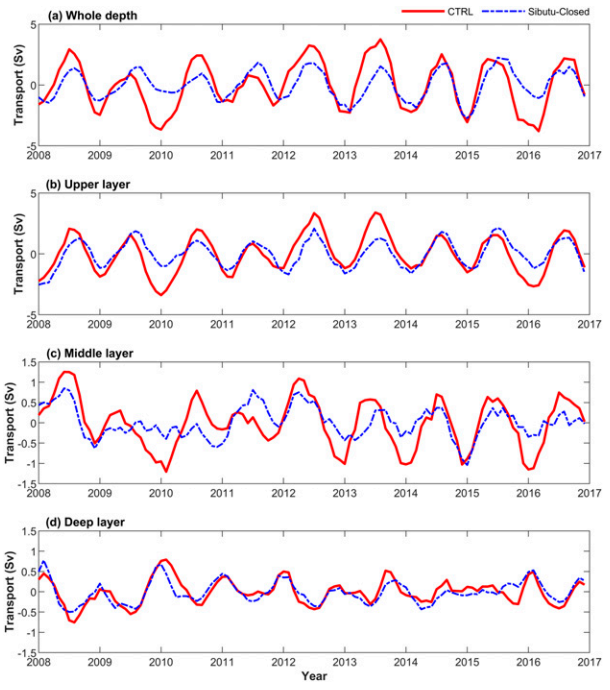

FIG. 9. Time series of Luzon Strait transport anomalies in each layer calculated from the control (solid red lines) and Sibutu_Closed experiments (dashed blue lines) for (a) whole-depth, (b) upper-layer (upper 900 m), (c) middle-layer, and (d) deep-layer volume transport; 3-month running means are applied to all time series to remove high-frequency variabilities.

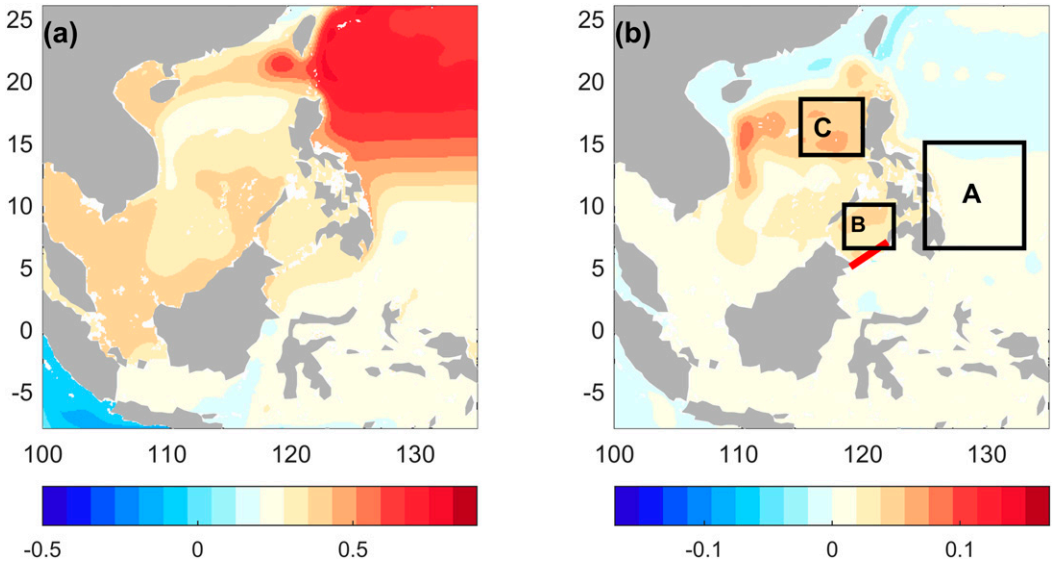

FIG. 10. (a) Time-averaged (2008–16) SSH (m) in the control experiment and (b) difference of the mean SSH between the Sibutu_Closed and control experiment. Boxes A, B, and C in (b) depict three regions in the western Pacific Ocean, the Sulu Sea, and the eastern SCS, respectively, that are used to calculate the regional mean SSH shown in Fig. 11, below.

also affected upon blocking the Mindoro–Sibutu pathway. The vertical structure of cyclonic–anticyclonic–cyclonic circulation also changes in both upper and middle layers. The cyclonic circulation in the upper layer is significantly weakened in the Sibutu_Closed experiment, as the upper layer thins, while the middle-layer anticyclonic circulation thickens and weakens relative to the control experiment (Fig. 8a). The upper layer becomes thinner in response to decrease the downward velocity within the upper layer (Fig. 8b). This confirms that a weakened vertical coupling between the upper and middle layers can induce a horizontal gradient of interface elevation to modulate the circulation in middle layer (Quan and Xue 2018).

With changes on vertical structure of the SCS circulation, the zonal velocity in Luzon Strait also experiences significant changes. Figure 8c shows the mean zonal velocity profile in the Luzon Strait, indicating the westward inflow from the surface to about 900 m, eastward outflow from 900 to about 2100 m, and westward inflow below 2100 m in the control experiment. This is consistent with the vertical structure of SCS circulation, which indicates that the multilayer circulation is significantly related to the sandwich-like velocity pattern in the Luzon Strait. From the control experiment, the total transport through Luzon Strait is −4.4 Sv, with layer-integrated transport of −5.0, 2.6, and −2.0 Sv in the upper (inflow), middle (outflow), and deep (inflow) layers, respectively. This result is consistent with previous studies based on both observations and models with the layer-integrated transport ranging from −10 to −3.5 Sv, from 0.22 to 5 Sv, and from −2 to −0.22 Sv in the upper, middle, and deep layers, respectively (e.g., Tian et al. 2006; Yuan et al. 2008; Xu and Oey 2014; Gan et al. 2016). The whole-depth Luzon Strait transport in the Sibutu_Closed experiment is −1.2 Sv, with −1.3, 2.1, and −2.0 Sv in upper, middle, and deep layers, respectively. Using the control experiment as a reference, closing the Mindoro–Sibutu pathway reduces Luzon Strait inflow transport by about 75%, especially in surface and subsurface layers. It appears that Luzon Strait inflow and the Mindoro–Sibutu outflow are linked via the basin-scale cyclonic circulation in surface and subsurface layers. The coupling of the SCS circulation between upper and middle layers plays an important role in weakening the middle-layer circulation in the Sibutu_Closed experiment.

c. *Sea level changes of the eastern SCS and relationship with Luzon Strait inflow*

The SCS general circulation partly driven by the inflow at Luzon Strait (an upstream site) flows counterclockwise to southeast of the SCS with the Mindoro–Sibutu pathway as the downstream. Water exchanges between the western Pacific Ocean and the SCS through Luzon Strait and the Mindoro–Sibutu pathway adjust the sea level variations in the eastern and northern SCS, which plays an important role in the SCS circulation and water properties (Xue et al. 2004; Zheng et al. 2007; Nan et al. 2013; Wu 2013). Previous studies have noted that sea level changes in the eastern SCS are highly correlated with interannual variability of the western Pacific Ocean sea level fluctuations around the Philippine coast (Liu et al. 2011; Zhuang et al. 2013). On interannual time scale, the Mindoro–Sibutu pathway contributes significantly to variability of Luzon Strait inflow and the SCSTF (Gordon et al. 2012; Yu and Qu 2013; Wei et al. 2016). Based on the time series of Luzon Strait transport anomalies in different layers (Fig. 9) from the control and Sibutu_Closed experiments, the Luzon Strait inflow shows significant seasonal and interannual variabilities at all depths, especially in upper layer. After closing the Mindoro–Sibutu pathway, the transport anomalies in all layers changed significantly in the winter of 2009/10 and 2015/16, which illustrates the transmission of El Niño signals via the oceanic pathway.

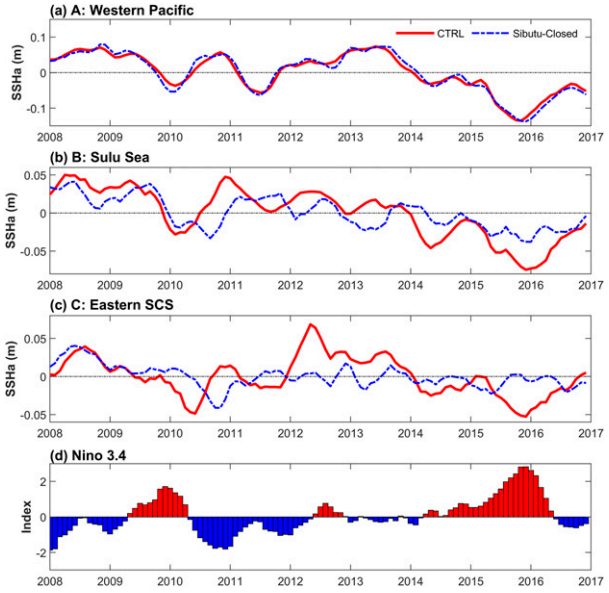

FIG. 11. Region-averaged SSH anomalies time series calculated from the Sibutu_Closed and control experiments over the three boxes in Fig. 10b: (a) region A, western Pacific Ocean; (b) region B, Sulu Sea; and (c) region C, the eastern SCS. Also shown is (d) Niño-3.4 index. The seasonal variations of all SSH anomalies time series are removed.

As a useful indicator of upper-ocean circulation, the sea surface height (SSH) anomalies are analyzed to further illustrate the impact of the Mindoro–Sibutu pathway on Luzon Strait inflow and SCS multilayer circulation. ENSO is known to excite westward-propagating Rossby waves. In particular, during an El Niño event, westward-propagating off-equatorial upwelling Rossby waves with associated negative SSH anomalies and shallow thermocline depth are generated by wind anomalies (Clarke 2008). The first baroclinic mode Rossby waves (with a speed of about 1 m s^{-1}), usually originated from midtropical longitudes of the Pacific Ocean, centered near 5°N. Previous studies (Alexander et al. 2010; Liu et al. 2011; Zhuang et al. 2013) have indicated that the wind-driven baroclinic Rossby waves excite coastal Kelvin waves when they arrive at the eastern Philippine coast, about 3 months after generation.

The time-averaged (2008–16) SSH (Fig. 10) in the control experiment and the difference between the Sibutu_Closed and control experiments, show that the sea level in the eastern SCS is increased by about 2–5 cm in the Sibutu_Closed experiment. We further chose three boxes (Fig. 10b) in the western Pacific Ocean, the Sulu Sea and the eastern SCS to calculate area mean SSH anomaly time series (Fig. 11). After removing the 9-yr mean seasonal cycle, all SSH anomalies time series show ENSO-related interannual variability, negative or positive SSH anomalies during El Niño or La Niña years, respectively. In the control experiment, SSH anomalies in the western Pacific Ocean and the Sulu Sea show the maximum negative correlation coefficients of −0.64 and −0.78 (99% significance level) to Niño-3.4 index at 1- and 3-month lags (Fig. 12). The SSH anomalies in the eastern SCS are negatively (−0.6) correlated with Niño-3.4 index with a 4-month lag, and they lag the sea level changes in the Sulu Sea and western Pacific Ocean by about 1 month.

Closing the Mindoro–Sibutu pathway induces significant changes of the SSH in the Sulu Sea and the eastern SCS. The

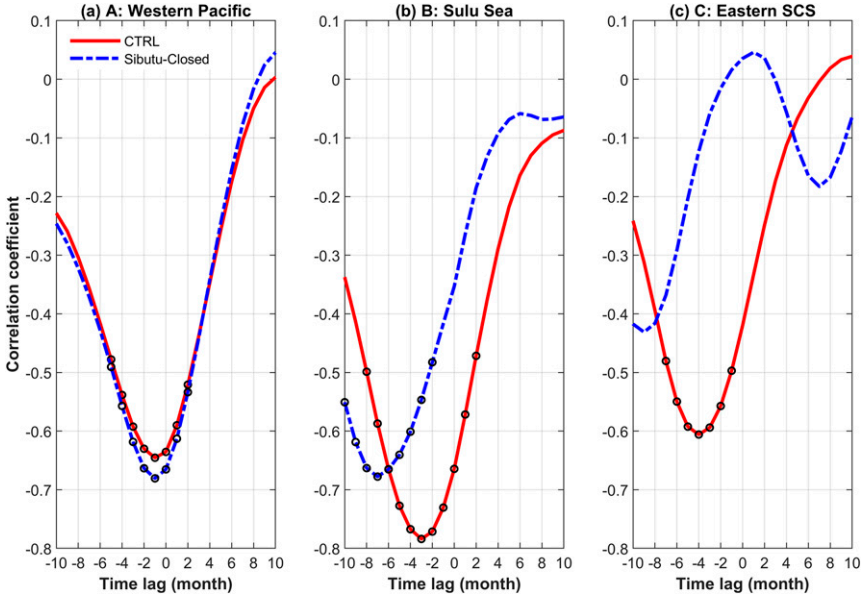

FIG. 12. Lead and lag correlations between Niño-3.4 index and SSH anomalies in three regions. Negative lag time means Niño-3.4 leading. Black open circles are above the 95% significance level as determined using an effective degree of freedom.

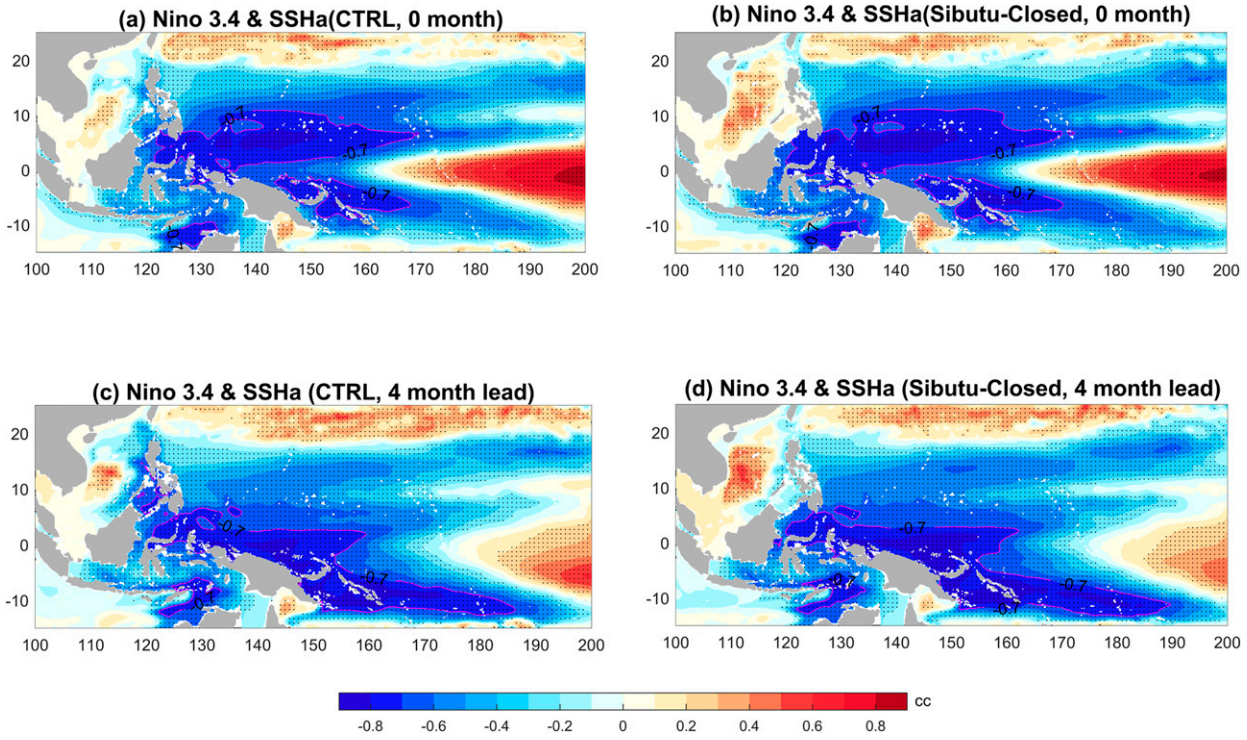

FIG. 13. Map view of correlations coefficients between Niño-3.4 index and SSH anomalies in the Pacific Ocean: (a),(b) zero lag correlations and (c),(d) 4-month lead of Niño-3.4 in the (left) control experiment and (right) Sibutu_Closed experiment. Stippling indicates significance above the 95% significance level as determined using an effective degree of freedom.

eastern SCS sea level is increased significantly during the winters of 2009/10 and 2015/16 (two El Niño events, Fig. 11c). The correlation coefficient between the Sulu Sea SSH anomalies and Niño-3.4 index reduces to −0.55 with 3-month lag, while the eastern SCS almost has no relationship with the Niño-3.4 index (Fig. 12c). The map views of correlation coefficients between SSH anomalies and Niño-3.4 index (Fig. 13) show that negative correlation coefficients of more than −0.7 penetrate into the eastern SCS along the coast of Philippine Islands after 4 months of ENSO mature phase in the control experiment, whereas the negative correlation extension is absent in the Sibutu_Closed experiment. This suggests that the oceanic waves can project the ENSO signal through the Mindoro–Sibutu pathway to modulate SSH in the eastern SCS. Hence, Luzon Strait is downstream of the Mindoro–Sibutu pathway in terms of oceanic wave propagation, but upstream relative to the SCS throughflow.

The Hovmöller diagram of SSH anomalies along the Philippine coast from the control and sensitivity experiments (Fig. 14) provide a view of oceanic wave propagation around the Philippine Archipelago. It is clearly shown that Rossby waves, originated in the middle tropical Pacific Ocean, propagate from station 1 to 10, and then excite Kelvin waves around the Philippine Archipelago through the Sulawesi Sea, then the Sula Sea via the Mindoro–Sibutu pathway to arrive at the eastern SCS. This propagation is interrupted by closing the Mindoro–Sibutu pathway while closing Luzon Strait has little impacts (not shown). There is a sharp decrease in wave energy around station 14 just before the coast of Mindanao, which may be induced by rapid southward and then eastward energy propagation associated with strong nonlinear processes of western boundary currents upon reaching the boundary (Wang and Yuan 2012, 2014). The SSH anomalies between the Sibutu_Closed and control experiments indicate that the interannual time-scale wave signals are significantly blocked when the Mindoro–Sibutu pathway is closed, while the remaining season cycle in the eastern SCS (stations 24–27) is due to local forcing. This suggests that the oceanic waves can convey ENSO signal by modulating the SSH in the eastern SCS through the Mindoro–Sibutu pathway.

The composite differences of the multilayer circulation between El Niño years (2009/10, 2015/16) and the 9-yr mean from the control and Sibutu_Closed experiments are shown in Fig. 15. In the control experiment, stronger Kuroshio intrusion currents in Luzon Strait during El Niño years produce a southward flow anomaly in the eastern SCS to the Mindoro–Sibutu pathway, which enhance the cyclonic circulation in the surface layer and subsurface layer. As a result of vertical coupling, the anticyclonic circulation of the middle layer also becomes stronger. By closing the Mindoro–Sibutu pathway in the Sibutu_Closed experiment, a significant weakening of the cyclonic circulation in surface layer is exhibited since there is less intrusion from Kuroshio in Luzon Strait. The subsurface and middle layers also experience slight weakening during El Niño years. The above analyses suggest that the oceanic wave signals associate with

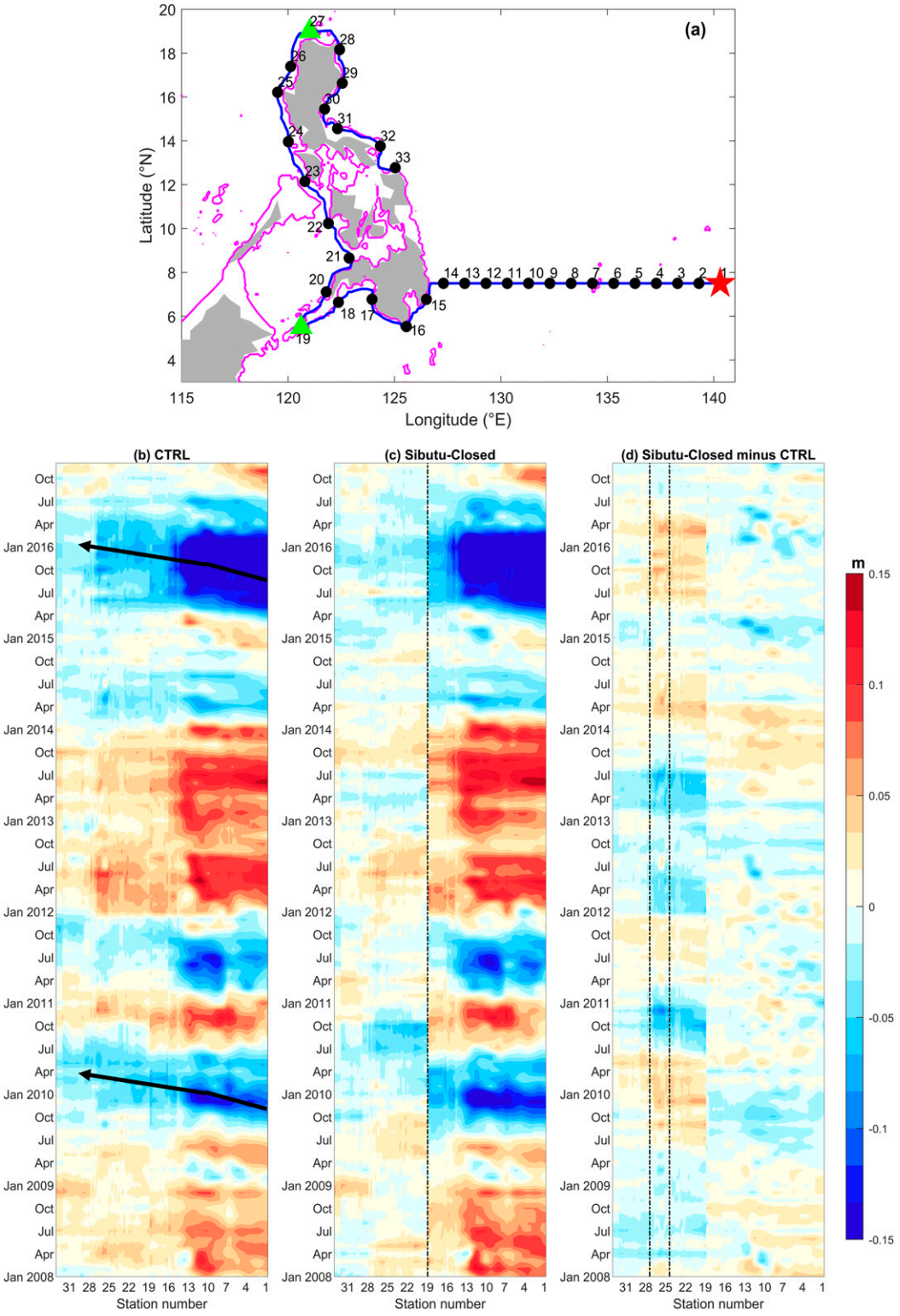

FIG. 14. (a) Stations used to depict time evolutions of the SSH anomalies (m). Time–station diagrams of monthly SSH anomalies from (b) the control and (c) Sibutu_Closed sensitivity experiments. The black arrows in (b) indicate the propagation of primary oceanic waves, and the black dashed line in (c) show the Sibutu Passage station 19. (d) The difference of SSH between the Sibutu_Closed and control experiments. The black dashed lines highlight the stations from 24 to 27, located in the eastern SCS. The difference is for SSH anomalies between the Sibutu_Closed and control experiments (Sibutu_Closed minus control).

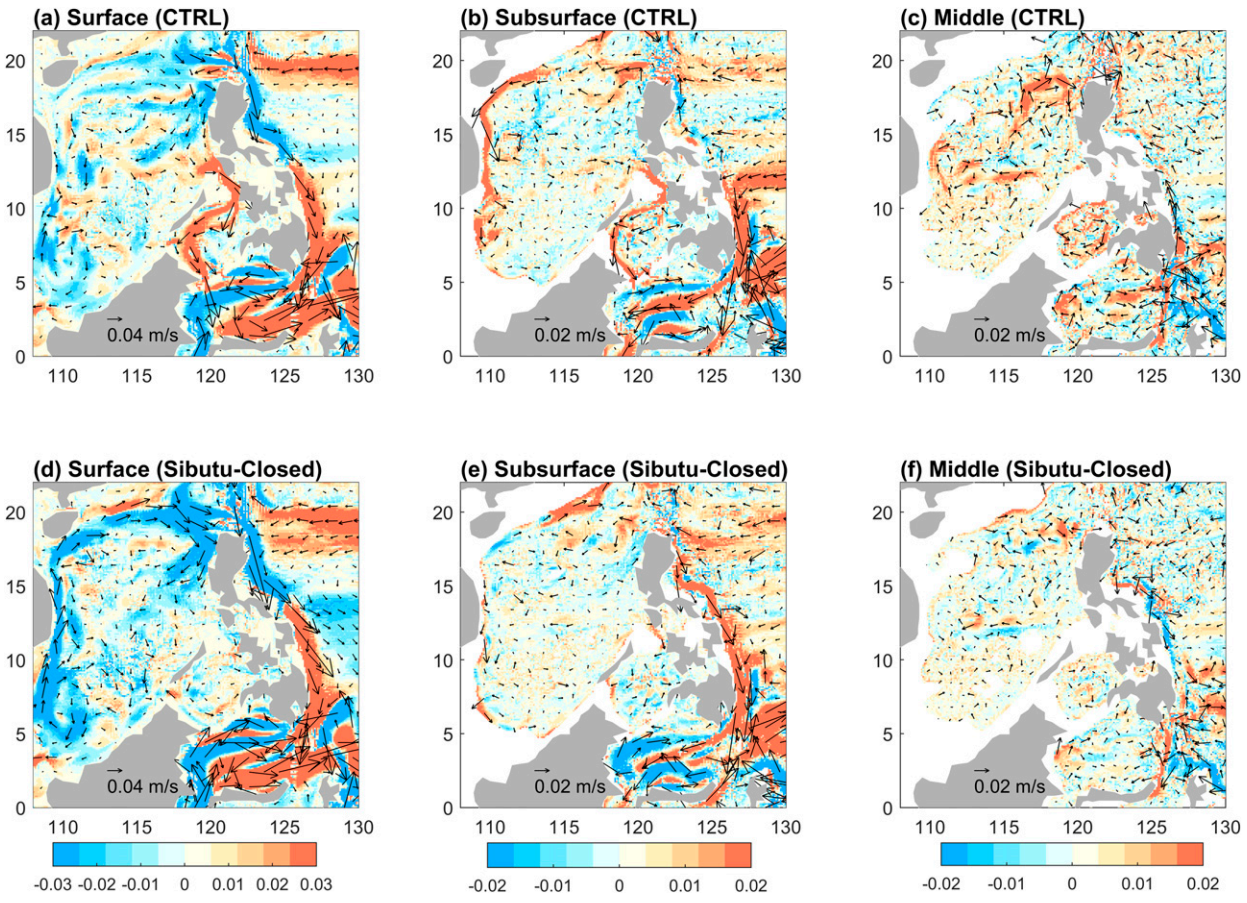

FIG. 15. Composite difference of depth-averaged velocity ($m\,s^{-1}$) of each layer between El Niño years (2009/10, 2015/16) and 9-yr mean (2008–16) from control run and the Sibutu_Closed experiment, i.e., El Niño years minus 9-yr mean shown in Figs. 4 and 7: (a) surface layer, (b) subsurface layer, (c) middle layer for control, and (d)–(f) for the Sibutu_Closed experiment. Shading represents value anomalies of velocity. Note that the color bars on the bottom of different panels have different scales.

ENSO may affect the SCS multilayer circulation by modulating the Luzon Strait inflow via the sea level in the eastern SCS.

4. Summary and discussions

In this study, using a high-resolution regional ocean model, the impact of the Mindoro–Sibutu pathway on the SCS multilayer circulation and Luzon Strait inflow is examined. After closing the Sibutu Strait (the Sibutu_Closed experiment), the cyclonic–anticyclonic–cyclonic structure of SCS multilayer circulation is weakened as Luzon Strait intrusion is reduced by 75%, from −4.4 to −1.2 Sv. Closing the Mindoro–Sibutu pathway also affects anticyclonic circulation in middle layer. The upper and middle layers respectively become thinner and thicker in the Sibutu_Closed experiment. There is no significant change in deep layer in the Sibutu_Closed experiment. The Mindoro–Sibutu pathway affects the Luzon Strait inflow by modulating sea level over the eastern SCS that adjusts the pressure gradient between east and west of Luzon Strait. The Mindoro–Sibutu pathway is the downstream pathway of SCS throughflow, but it is the upstream gateway for ocean waves propagating from the western Pacific Ocean to the eastern SCS. The interannual time-scale wave signals are significantly blocked by closing the Mindoro–Sibutu pathway. The ocean waves conveying ENSO signal through modulating the SSH and propagate into SCS via the Mindoro–Sibutu pathway.

By closing the Luzon Strait, the cyclonic circulation in the surface and subsurface layer weakens by more than half, with velocity differences between the Luzon_Closed and control experiments being about $0.1\,m\,s^{-1}$ in the surface layer as the remaining cyclonic circulation is driven by wind stress. The cyclonic circulation in the deep layer almost disappears since there is no overflow from Luzon Strait into the deep SCS (Fig. S3d in the online supplemental material). However, the vertical structure of cyclonic–anticyclonic–cyclonic circulation still exists with much smaller vorticity values because the abyssal circulation needs several decades to reach equilibrium (Wang et al. 2019). The SCS basin-scale velocity of anticyclonic circulation in the middle layer is reduced by more than $0.02\,m\,s^{-1}$, about 20% of the mean middle-layer circulation. The SCS domain-integrated vorticity based on the Luzon_Closed experiment indicates that the anticyclonic circulation in the middle layer remains, but only at about 1/3 of the strength (Fig. S4 in the online supplemental material). The sea level of

whole SCS domain is decreased more than 5 cm if both Luzon Strait and Sibutu Passage are closed, while the SSH in the whole western Pacific Ocean and Indonesian Seas are increased by about 2–5 cm (not shown).

The western boundary currents of the Pacific Ocean are also altered by closing the Mindoro–Sibutu pathway, with a stronger Mindanao Current and weaker Kuroshio along the Philippine coast in surface layer (Fig. S5e in the online supplemental material). Metzger and Hurlburt (1996) have indicated that transport of Mindoro Strait can modulate the NEC bifurcation, and the Mindoro–Sibutu pathway also plays a role in modifying the mean circulation pattern in the western Pacific Ocean. Closing only the Luzon Strait also induced a weaker surface Kuroshio and stronger Mindanao Current (Fig. S5a). There are southward current anomalies originated from south of Luzon Strait along the east coast of Philippines in surface and subsurface layers when either Luzon Strait or the Mindoro–Sibutu pathway was closed (Figs. S5a,e,i), which implies that the Mindoro–Sibutu pathway can also influence the NEC bifurcation and boundary currents in the western Pacific Ocean.

As we have indicated that the Mindoro Strait–Sibutu Passage is the key pathway for ocean wave propagation from western Pacific Ocean into the SCS. The Mindoro–Sibutu pathway also plays an important role in modulating the multilayer circulation of SCS, since it is the key downstream flow to Luzon Strait inflow and affects the Luzon Strait inflow by modulating the sea level over eastern SCS. The sea level changes of SCS and the western Pacific Ocean act as an important factor of SCS throughflow, as well as the Indonesian Throughflow. As an important branch of SCS throughflow, the flow through the Mindoro–Sibutu pathway plays a role on freshwater plug in Sulawesi Sea to modulate the interannual variability of Indonesian Throughflow (Gordon et al. 2012; Wei et al. 2016; Li et al. 2019). The mean transport through the Mindoro Strait and Sibutu Passage based on ATOP model is southward at 2.7 and 2.9 Sv, respectively. Although these numbers agree with previous model estimates, the sill depth of the Sibutu Passage in ATOP model is about 400 m (Fig. 2), which is believed to be deeper than the sill depth in the real world. Cross section of the mean flow through the Sibutu Passage shows the strongest southward flow around the 300-m depth. As such, the deeper sill depth of Sibutu Passage may affect the modeled circulation in the Sulu Sea. However, there is no in situ observation of velocity as yet in the Sibutu Passage with which to compare the ATOP model simulation. In addition, since the PhilEx project only observed in the Mindoro Strait for one year during 2008, which was a strong La Niña year with a less than usual transport through the Mindoro Strait. In addition, as Sprintall et al. (2012) mentioned, the mooring was located in the east of the main channel and thus might not capture the strongest southward flow. Longer time observations are needed to investigate the variability of the Mindoro–Sibutu pathway flow in different time scales and to verify and improve the accuracy of model simulations for this region.

Acknowledgments. We thank the anonymous reviewers for their insightful and constructive comments. We also thank the Advanced Taiwan Ocean Prediction model group (http://mpi-pom.ihs.ncu.edu.tw) for providing codes for the model simulations used in this study. The climatological temperature and salinity data for model open boundary conditions are from the *World Ocean Atlas* (*WOA*; https://climatedataguide.ucar.edu/climate-data/world-ocean-atlas-2013-woa13). The CCMP data are available online (http://www.remss.com/measurements/ccmp/). This work was supported by National Natural Science Foundation of China (Grant 41906004), the Strategic Priority Research Program of the Chinese Academy of Sciences (Project XDB420000000), Guangdong Basic and Applied Basic Research Foundation (Grant 2019A1515011245), State Key Laboratory of Tropical Oceanography, South China Sea Institute of Oceanology, Chinese Academy of Sciences (Project LTO1914), and Guangdong Province Key Area Research and Development Project (Grant 2020B1111020003). The funding for author Gordon is derived from the Climate Program Office, Office of Climate Observation, National Oceanic and Atmospheric Administration, U.S. Department of Commerce. The statements, findings, conclusions, and recommendations are those of the author(s) and do not necessarily reflect the views of the National Oceanic and Atmospheric Administration or the Department of Commerce.

REFERENCES

Alexander, M. A., D. J. Vimont, P. Chang, and J. D. Scott, 2010: The impact of extratropical atmospheric variability on ENSO: Testing the seasonal footprinting mechanism using coupled model experiments. *J. Climate*, **23**, 2885–2901, https://doi.org/10.1175/2010JCLI3205.1.

Berntsen, J., and L. Y. Oey, 2010: Estimation of the internal pressure gradient in σ-coordinate ocean models: Comparison of second-, fourth-, and sixth-order schemes. *Ocean Dyn.*, **60**, 317–330, https://doi.org/10.1007/s10236-009-0245-y.

Cai, Z., and J. Gan, 2019: Coupled external-internal dynamics of layered circulation in the South China Sea: A modeling study. *J. Geophys. Res. Oceans*, **124**, 5039–5053, https://doi.org/10.1029/2019JC014962.

——, ——, Z. Liu, C. R. Hui, and J. Li, 2020: Progress on the formation dynamics of the layered circulation in the South China Sea. *Prog. Oceanogr.*, **181**, 102246, https://doi.org/10.1016/j.pocean.2019.102246.

Chen, X., B. Qiu, X. Cheng, Y. Qi, and Y. Du, 2015: Intra-seasonal variability of Pacific-origin sea level anomalies around the Philippine Archipelago. *J. Oceanogr.*, **71**, 239–249, https://doi.org/10.1007/s10872-015-0281-9.

Chu, P. C., N. L. Edmons, and C. Fan, 1999: Dynamical mechanisms for the South China Sea seasonal circulation and thermohaline variabilities. *J. Phys. Oceanogr.*, **29**, 2971–2989, https://doi.org/10.1175/1520-0485(1999)029<2971:DMFTSC>2.0.CO;2.

Clarke, A. J., 2008: *An Introduction to the Dynamics of El Niño and the Southern Oscillation*. Academic Press, 308 pp.

Du, Y., and T. Qu, 2010: Three inflow pathways of the Indonesian throughflow as seen from the simple ocean data assimilation. *Dyn. Atmos. Oceans*, **50**, 233–256, https://doi.org/10.1016/j.dynatmoce.2010.04.001.

Fang, G., and Coauthors, 2010: Volume, heat, and freshwater transports from the South China Sea to Indonesian seas in the boreal winter of 2007–2008. *J. Geophys. Res.*, **115**, C12020, https://doi.org/10.1029/2010JC006225.

Gan, J., H. Li, E. N. Curchitser, and D. B. Haidvogel, 2006: Modeling South China Sea circulation: Response to seasonal forcing regimes. *J. Geophys. Res.*, **111**, C06034, https://doi.org/10.1029/2005JC003298.

——, Z. Liu, and C. R. Hui, 2016: A three-layer alternating spinning circulation in the South China Sea. *J. Phys. Oceanogr.*, **46**, 2309–2315, https://doi.org/10.1175/JPO-D-16-0044.1.

Gordon, A. L., and C. L. Villanoy, 2011: The oceanography of the Philippine Archipelago: Introduction to the special issue. *Oceanography*, **24**, 13, https://doi.org/10.5670/oceanog.2011.13.

——, J. Sprintall, and A. Ffield, 2011: Regional oceanography of the Philippine Archipelago. *Oceanography*, **24**, 14–27, https://doi.org/10.5670/oceanog.2011.01.

——, B. A. Huber, E. J. Metzger, R. D. Susanto, H. E. Hurlburt, and T. R. Adi, 2012: South China Sea throughflow impact on the Indonesian throughflow. *Geophys. Res. Lett.*, **39**, L11602, https://doi.org/10.1029/2012GL052021.

Hu, J., H. Kawamura, H. Hong, and Y. Qi, 2000: A review on the currents in the South China Sea: Seasonal circulation, South China Sea warm current and Kuroshio intrusion. *J. Oceanogr.*, **56**, 607–624, https://doi.org/10.1023/A:1011117531252.

Hu, X., and Coauthors, 2019: Interannual variability of the Sulawesi Sea circulation forced by Indo-Pacific planetary waves. *J. Geophys. Res. Oceans*, **124**, 1616–1633, https://doi.org/10.1029/2018JC014356.

Hurlburt, H. E., E. J. Metzger, J. Sprintall, S. N. Riedlinger, R. A. Arnone, T. Shinoda, and X. Xu, 2011: Circulation in the Philippine archipelago simulated by 1/12° and 1/25° global HYCOM and EAS NCOM. *Oceanography*, **24**, 28–47, https://doi.org/10.5670/oceanog.2011.02.

Lan, J., N. Zhang, and Y. Wang, 2013: On the dynamics of the South China Sea deep circulation. *J. Geophys. Res. Oceans*, **118**, 1206–1210, https://doi.org/10.1002/jgrc.20104.

——, Y. Wang, F. Cui, and N. Zhang, 2015: Seasonal variation in the South China Sea deep circulation. *J. Geophys. Res. Oceans*, **120**, 1682–1690, https://doi.org/10.1002/2014JC010413.

Li, M., J. Wei, D. Wang, A. L. Gordon, S. Yang, P. Malanotte-Rizzoli, and G. Jiang, 2019: Exploring the importance of the Mindoro-Sibutu Pathway to the upper-layer circulation of the South China Sea and the Indonesian Throughflow. *J. Geophys. Res. Oceans*, **124**, 5054–5066, https://doi.org/10.1029/2018JC014910.

Liu, Q., H. Yang, and Z. Liu, 2001: Seasonal features of the Sverdrup circulation in the South China Sea. *Prog. Nat. Sci.*, **11**, 202–206.

——, M. Feng, and D. Wang, 2011: ENSO-induced interannual variability in the southeastern South China Sea. *J. Oceanogr.*, **67**, 127–133, https://doi.org/10.1007/s10872-011-0002-y.

——, R. Huang, and D. Wang, 2012: Implication of the South China Sea throughflow for the interannual variability of the regional upper-ocean heat content. *Adv. Atmos. Sci.*, **29**, 54–62, https://doi.org/10.1007/s00376-011-0068-x.

Mears, C. A., and Coauthors, 2019: A near real time version of the Cross Calibrated Multiplatform (CCMP) ocean surface wind velocity data set. *J. Geophys. Res. Oceans*, **124**, 6997–7010, https://doi.org/10.1029/2019JC015367.

Mellor, G. L., and T. Yamada, 1982: Development of a turbulence closure model for geophysical fluid problems. *Rev. Geophys.*, **20**, 851–875, https://doi.org/10.1029/RG020i004p00851.

Metzger, E. J., and H. E. Hurlburt, 1996: Coupled dynamics of the South China Sea, the Sulu Sea, and the Pacific Ocean. *J. Geophys. Res.*, **101**, 12 331–12 352, https://doi.org/10.1029/95JC03861.

Nan, F., H. Xue, F. Chai, L. Shi, M. Shi, and P. Guo, 2011: Identification of different types of Kuroshio intrusion into the South China Sea. *Ocean Dyn.*, **61**, 1291–1304, https://doi.org/10.1007/s10236-011-0426-3.

——, ——, ——, D. Wang, F. Yu, M. Shi, P. Guo, and P. Xiu, 2013: Weakening of the Kuroshio intrusion into the South China Sea over the past two decades. *J. Climate*, **26**, 8097–8110, https://doi.org/10.1175/JCLI-D-12-00315.1.

——, ——, and F. Yu, 2015: Kuroshio intrusion into the South China Sea: A review. *Prog. Oceanogr.*, **137**, 314–333, https://doi.org/10.1016/j.pocean.2014.05.012.

Oey, L.-Y., and P. Chen, 1992a: A nested-grid ocean model: With application to the simulation of meanders and eddies in the Norwegian Coastal Current. *J. Geophys. Res.*, **97**, 20 063–20 086, https://doi.org/10.1029/92JC01991.

——, and C. Ping, 1992b: A model simulation of circulation in the northeast Atlantic shelves and seas. *J. Geophys. Res.*, **97**, 20 087–20 115, https://doi.org/10.1029/92JC01990.

Oey, L., Y. L. Chang, Y. C. Lin, M. C. Chang, F. Xu, and H. F. Lu, 2013: ATOP -The advanced Taiwan ocean prediction system based on the mpiPOM. Part 1: Model descriptions, analyses and results. *Terr. Atmos. Ocean. Sci.*, **24**, 137–158, https://doi.org/10.3319/TAO.2012.09.12.01(Oc).

Oey, L. Y., Y. L. Chang, Y. C. Lin, M. C. Chang, S. Varlamov, and Y. Miyazawa, 2014: Cross flows in the Taiwan strait in winter. *J. Phys. Oceanogr.*, **44**, 801–817, https://doi.org/10.1175/JPO-D-13-0128.1.

Qu, T., 2000: Upper-layer circulation in the South China Sea. *J. Phys. Oceanogr.*, **30**, 1450–1460, https://doi.org/10.1175/1520-0485(2000)030<1450:ULCITS>2.0.CO;2.

——, and Y. T. Song, 2009: Mindoro Strait and Sibutu Passage transports estimated from satellite data. *Geophys. Res. Lett.*, **36**, L09601, https://doi.org/10.1029/2009GL037314.

——, Y. Y. Kim, M. Yaremchuk, T. Tuzuka, A. Ishida, and T. Yamagata, 2004: Can Luzon Strait transport play a role in conveying the impact of ENSO to the South China Sea? *J. Climate*, **17**, 3644–3657, https://doi.org/10.1175/1520-0442(2004)017<3644:CLSTPA>2.0.CO;2.

——, Y. Du, G. Meyers, A. Ishida, and D. Wang, 2005: Connecting the tropical Pacific with Indian Ocean through South China Sea. *Geophys. Res. Lett.*, **32**, L24609, https://doi.org/10.1029/2005GL024698.

——, ——, and H. Sasaki, 2006: South China Sea throughflow: A heat and freshwater conveyor. *Geophys. Res. Lett.*, **33**, L23617, https://doi.org/10.1029/2006GL028350.

——, Y. T. Song, and T. Yamagata, 2009: An introduction to the South China Sea throughflow: Its dynamics, variability, and application for climate. *Dyn. Atmos. Oceans*, **47**, 3–14, https://doi.org/10.1016/j.dynatmoce.2008.05.001.

Quan, Q., and H. Xue, 2018: Layered model and insights into the vertical coupling of the South China Sea circulation in the upper and middle layers. *Ocean Modell.*, **129**, 75–92, https://doi.org/10.1016/j.ocemod.2018.06.006.

——, and ——, 2019: Influence of abyssal mixing on the multi-layer circulation in the South China Sea. *J. Phys. Oceanogr.*, **49**, 3045–3060, https://doi.org/10.1175/JPO-D-19-0020.1.

——, ——, H. Qin, X. Zeng, and S. Peng, 2016: Features and variability of the South China Sea western boundary current from 1992 to 2011. *Ocean Dyn.*, **66**, 795–810, https://doi.org/10.1007/s10236-016-0951-1.

Shu, Y., H. Xue, D. Wang, F. Chai, Q. Xie, J. Yao, and J. Xiao, 2014: Meridional overturning circulation in the South China Sea envisioned from the high-resolution global reanalysis data

GLBa0.08. *J. Geophys. Res. Oceans*, **119**, 3012–3028, https://doi.org/10.1002/2013JC009583.

Smagorinsky, J., 1963: General circulation experiments with the primitive equations: I The basic experiment. *Mon. Wea. Rev.*, **91**, 99–164, https://doi.org/10.1175/1520-0493(1963)091<0099:GCEWTP>2.3.CO;2.

Sprintall, J., A. L. Gordon, P. Flament, and C. L. Villanoy, 2012: Observations of exchange between the South China Sea and the Sulu Sea. *J. Geophys. Res.*, **117**, C05036, https://doi.org/10.1029/2011JC007610.

Su, J., 2004: Overview of the South China Sea circulation and its influence on the coastal physical oceanography outside the Pearl River Estuary. *Cont. Shelf Res.*, **24**, 1745–1760, https://doi.org/10.1016/j.csr.2004.06.005.

Susanto, R. D., Z. Wei, R. T. Adi, B. Fan, S. Li, and G. Fang, 2013: Observations of the Karimata Strait throughflow from December 2007 to November 2008. *Acta Oceanol. Sin.*, **32**, 1–6, https://doi.org/10.1007/s13131-013-0307-3.

Tian, J. W., and T. D. Qu, 2012: Advances in research on the deep South China Sea circulation. *Chin. Sci. Bull.*, **57**, 3115–3120, https://doi.org/10.1007/s11434-012-5269-x.

——, Q. Yang, X. Liang, L. Xie, D. Hu, F. Wang, and T. D. Qu, 2006: Observation of Luzon Strait transport. *Geophys. Res. Lett.*, **33**, L19607, https://doi.org/10.1029/2006GL026272.

Tozuka, T., T. Qu, and T. Yamagata, 2007: Dramatic impact of the South China Sea on the Indonesian throughflow. *Geophys. Res. Lett.*, **34**, L12612, https://doi.org/10.1029/2007GL030420.

——, ——, Y. Masumoto, and T. Yamagata, 2009: Impacts of the South China Sea Throughflow on seasonal and interannual variations of the Indonesian Throughflow. *Dyn. Atmos. Oceans*, **47**, 73–85, https://doi.org/10.1016/j.dynatmoce.2008.09.001.

Tsui, I. F., and C. R. Wu, 2012: Variability analysis of Kuroshio intrusion through Luzon Strait using growing hierarchical self-organizing map. *Ocean Dyn.*, **62**, 1187–1194, https://doi.org/10.1007/s10236-012-0558-0.

Wang, D., Q. Liu, R. X. Huang, Y. Du, and T. Qu, 2006: Interannual variability of the South China Sea throughflow inferred from wind data and an ocean data assimilation product. *Geophys. Res. Lett.*, **33**, L14605, https://doi.org/10.1029/2006GL026316.

——, and Coauthors, 2019: Advances in research of the mid-deep South China Sea circulation. *Sci. China Earth Sci.*, **62**, 1992–2004, https://doi.org/10.1007/s11430-019-9546-3.

Wang, G., D. Chen, and J. Su, 2006: Generation and life cycle of the dipole in the South China Sea summer circulation. *J. Geophys. Res.*, **111**, C06002, https://doi.org/10.1029/2005JC003314.

——, S. P. Xie, T. Qu, and R. X. Huang, 2011: Deep South China Sea circulation. *Geophys. Res. Lett.*, **38**, L05601, https://doi.org/10.1029/2010GL046626.

——, R. X. Huang, J. Su, and D. Chen, 2012: The effects of thermohaline circulation on wind-driven circulation in the South China Sea. *J. Phys. Oceanogr.*, **42**, 2283–2296, https://doi.org/10.1175/JPO-D-11-0227.1.

Wang, Z., and D. Yuan, 2012: Nonlinear dynamics of two western boundary currents colliding at a gap. *J. Phys. Oceanogr.*, **42**, 2030–2040, https://doi.org/10.1175/JPO-D-12-05.1.

——, and ——, 2014: Multiple equilibria and hysteresis of two unequal-transport western boundary currents colliding at a gap. *J. Phys. Oceanogr.*, **44**, 1873–1885, https://doi.org/10.1175/JPO-D-13-0234.1.

Wei, J., M. T. Li, P. Malanotte-Rizzoli, A. L. Gordon, and D. X. Wang, 2016: Opposite variability of Indonesian Throughflow and South China Sea Throughflow in the Sulawesi Sea. *J. Phys. Oceanogr.*, **46**, 3165–3180, https://doi.org/10.1175/JPO-D-16-0132.1.

Wu, C. R., 2013: Interannual modulation of the Pacific Decadal Oscillation (PDO) on the low-latitude western North Pacific. *Prog. Oceanogr.*, **110**, 49–58, https://doi.org/10.1016/j.pocean.2012.12.001.

Wyrtki, K., 1961: Physical Oceanography of the Southeast Asian waters. Scripps Institution of Oceanography NAGA Rep., Vol. 2, 195 pp.

Xu, F.-H., and L.-Y. Oey, 2014: State analysis using the Local Ensemble Transform Kalman Filter (LETKF) and the three-layer circulation structure of the Luzon Strait and the South China Sea. *Ocean Dyn.*, **64**, 905–923, https://doi.org/10.1007/s10236-014-0720-y.

Xue, H., F. Chai, N. Pettigrew, D. Xu, M. Shi, and J. Xu, 2004: Kuroshio intrusion and the circulation in the South China Sea. *J. Geophys. Res.*, **109**, C02017, https://doi.org/10.1029/2002JC001724.

Yang, J., and J. F. Price, 2000: Water-mass formation and potential vorticity balance in an abyssal ocean circulation. *J. Mar. Res.*, **58**, 789–808, https://doi.org/10.1357/002224000321358918.

Yu, K., and T. Qu, 2013: Imprint of the pacific decadal oscillation on the South China Sea throughflow variability. *J. Climate*, **26**, 9797–9805, https://doi.org/10.1175/JCLI-D-12-00785.1.

Yuan, D., 2002: A numerical study of the South China Sea deep circulation and its relation to the Luzon Strait transport. *Acta Oceanol. Sin.*, **2**, 36–51.

Yuan, Y., G. Liao, and C. Yang, 2008: The Kuroshio near the Luzon Strait and circulation in the northern South China Sea during August and September 1994. *J. Oceanogr.*, **64**, 777–788, https://doi.org/10.1007/s10872-008-0065-6.

Zheng, Z. W., C. R. Ho, and N. J. Kuo, 2007: Mechanism of weakening of west Luzon eddy during La Niña years. *Geophys. Res. Lett.*, **34**, L11604, https://doi.org/10.1029/2007GL030058.

Zhu, Y., J. Sun, Y. Wang, Z. Wei, D. Yang, and T. Qu, 2017: Effect of potential vorticity flux on the circulation in the South China Sea. *J. Geophys. Res. Oceans*, **122**, 6454–6469, https://doi.org/10.1002/2016JC012375.

——, ——, ——, S. Li, T. Xu, Z. Wei, and T. Qu, 2019: Overview of the multi-layer circulation in the South China Sea. *Prog. Oceanogr.*, **175**, 171–182, https://doi.org/10.1016/j.pocean.2019.04.001.

Zhuang, W., B. Qiu, and Y. Du, 2013: Low-frequency western Pacific Ocean sea level and circulation changes due to the connectivity of the Philippine archipelago. *J. Geophys. Res. Oceans*, **118**, 6759–6773, https://doi.org/10.1002/2013JC009376.

Zu, T., H. Xue, D. Wang, B. Geng, L. Zeng, Q. Liu, J. Chen, and Y. He, 2019: Interannual variation of the South China Sea circulation during winter: Intensified in the southern basin. *Climate Dyn.*, **52**, 1917–1933, https://doi.org/10.1007/s00382-018-4230-3.

——, D. Wang, Q. Wang, M. Li, J. Wei, B. Geng, Y. He, and J. Chen, 2020: A revisit of the interannual variation of the South China Sea upper layer circulation in summer: Correlation between the eastward jet and northward branch. *Climate Dyn.*, **54**, 457–471, https://doi.org/10.1007/s00382-019-05007-5.